ACS Sustainable Chemistry & Engineering

pubs.acs.org/journal/ascecg

Research Article

# Visible Light–Near-Infrared Dual-Band Electrochromic Device

Marco Pugliese,[‖] Riccardo Scarfiello,[‖] Carmela Tania Prontera, Roberto Giannuzzi,* Giuseppe Valerio Bianco, Giovanni Bruno, Sonia Carallo, Fabrizio Mariano, Antonio Maggiore, Luigi Carbone,* Giuseppe Gigli, and Vincenzo Maiorano

Cite This: *ACS Sustainable Chem. Eng.* 2023, 11, 9601−9612

Read Online

ACCESS | Metrics & More | Article Recommendations | Supporting Information

**ABSTRACT:** We herein propose a proof of concept of a full dual-band electrochromic (EC) device able to selectively modulate solar light between 300 and 1600 nm. Dual-band control was achieved by exploiting the complementarity and cooperation of two earth-abundant and nontoxic transition metal oxide nanocrystalline materials able to absorb two different spectral regions when electrochemically charged. The active materials were obtained through a microwave-based synthetic protocol able to produce massive amounts of ligand-free water-soluble $TiO_2$@$WO_{3-x}$ colloidal heterostructured nanocrystals. The inorganic heterostructures were deposited via a spray-coating airbrushing method. Graphene was adopted as a near-infrared (NIR) transparent material for the realization of conductive substrates. The nano-dimensions and stable solubility of active materials during the deposition process endorse the development of scattering-free nanostructured electrodes and high device transparency under open-circuit conditions, respectively. The spectro-electrochemical properties of the as-made nanostructured electrodes were evaluated in relation to pure $WO_{3-x}$ and $TiO_2$ single nanomaterials and a blend of these. The heterostructured architecture ensures a lower optical haze (around 8% of total radiation) as against the blend, contributing to improving the overall EC performance. The $TiO_2$@$WO_{3-x}$-based device shows 67% NIR shielding while preserving 60% of visible (VIS) transparency under cool-mode conditions and 89% screening of VIS and NIR radiation under the dark mode. These results represent an important step forward in the development of scalable dual-band EC devices.

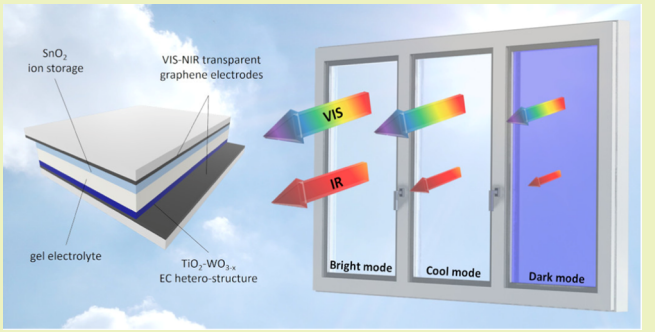


**KEYWORDS:** *electrochromic device, heterostructured $TiO_2$@$WO_{3-x}$ nanocrystals, near-infrared radiation, dual-band modulation, graphene electrode, spray coating*



## 1. INTRODUCTION

Buildings consume more than 40% of the world's energy and produce a third of global greenhouse gas emissions in both industrialized and developing countries.[1−3] This energy is mainly used for heating, ventilation, air-conditioning, and lighting (HVAC). In this context, windows represent one of the main building components to be considered to reduce energy needs/dissipation for HVAC, as a significant amount of heat and light is absorbed or lost through them.[4,5] An ideal window would provide pleasant glare-free lighting, excellent thermal insulation, and the ability to bring in infrared light when it is beneficial for heating but block it out when it would add to cooling loads.[6] Indeed, the near-infrared (NIR) region of the solar spectrum accounts for almost 50% of solar energy, so the ability to dynamically and selectively control the NIR radiation through windows has a significant impact on building thermal management and occupant comfort.[7] Moreover, an ideal window should also screen ultraviolet (UV) rays, which can damage skin and materials.

Electrochromic (EC) "smart windows" have emerged as a promising technology that can reversibly change their optical properties according to weather conditions and personal preferences.[8]

Many existing EC "smart windows" are capable of blocking both visible (VIS) and NIR radiation in the colored state without providing any spectral selectivity. Recently, the localized surface plasmon resonances (LSPRs) in transparent semiconductor oxides (ITO, AZO, IZO, FICO) have been exploited for the development of an active coating that can modulate NIR radiation without affecting VIS transmittance.[9−14]

Received: February 14, 2023
Revised: May 29, 2023
Published: June 15, 2023

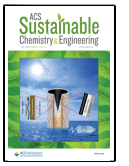

A step toward the development of a device for independent modulation of VIS and NIR radiation has been made by defect engineering EC materials.[15,16] In this class of materials, the introduction of defects, dopants, substituted atoms, or oxygen vacancies increases the density of free electrons and generates absorption in the NIR range due to LSPRs. Among them, $TiO_2$ doped with aliovalent metal atoms (Nb, Ta) has been evaluated as a material supporting LSPR absorption in the NIR range and modulation in the VIS range due to polaron formation.[17−19]

Oxygen vacancies have also been shown to enhance the performance of $TiO_2$ and $WO_3$, providing a simpler alternative for the development of dual-band EC materials compared to the approach of aliovalent doping of $TiO_2$ nanocrystals (NCs).[20,21] However, self-doping induced by oxygen deficiency improves the absorption in the NIR region due to the increased electron density and may be ineffective if the film preparation requires high aerobic-sintering temperatures such as 450 °C.[20]

Another approach for the development of a device for independent modulation of VIS and NIR radiation has been made through the combination of materials that can modulate the NIR region with those that modulate the VIS range of the electromagnetic spectrum. In particular, a nanocomposite obtained by dispersing ITO nanoparticles within an $NbO_x$ glass matrix was reported to modulate both spectral bands by controlling the applied voltage.[22] Three optical states were progressively achieved with the mentioned nanocrystal-in-glass coating by increasing the applied voltage: full transparency, selective NIR blocking, and both VIS and NIR blocking (broad band). However, despite having exhibited excellent results on a laboratory scale, these approaches present some challenges related to the industrial needs for scale-up. In particular, there are some issues associated with the scalability of NC synthesis and film deposition techniques. Although colloidal synthesis guarantees control over the shape, size, and composition of such NCs, this approach suffers from relatively low product concentrations and yields. In addition, NCs have organic capping around the particles, which must be removed to ensure good electrical contact between the particles in the film state. This can be done by using a high annealing temperature in air; however, this process can lead to partial melting of the nanostructure and possible changes of lattice structures and may result in the diffusion of dopant species. Another effective technique for the removal of the capping layer is ligand stripping and exchange.[23,24] The shortcomings of this technique are the difficulty in working with large thicknesses and the threat of etching the surface of the NCs. NCs take advantage of the improved surface-to-volume ratio, a condition that greatly enhances the kinetics of surface redox reactions and correspondingly fast switching times, and creates large surfaces for ion exchange.

In this study, we used the cooperative EC properties of graphene-based nanostructured electrodes whereby $TiO_2$ and $WO_{3-x}$ nanostructures are either combined within $TiO_2$@$WO_{3-x}$ nano-heterostructures or deposited out of a merely blended mixture. Both nanocrystalline breeds were obtained through microwave-assisted synthesis.[25] This approach revealed to be a valid and efficient alternative for dual-band EC device applications, circumventing the common issues for film production (e.g., substitutional doping stability and ligand stripping procedure). The microwave-assisted synthetic method has indisputable prerogatives (such as fast and homogeneous heating rates) that make the nanostructure production inexpensive, efficient, energy- and time-saving, and convenient to scale up, all of them being important requirements for industrially scaled production.[26] Since there are no long alkyl chain surfactants, the films can be treated by gentle annealing at 300 °C. Moreover, for the deposition of the thin film, airbrushing spray-coating of hydro-alcoholic solution directly onto a conductive substrate (ITO or graphene) was employed as a low-cost and large-area deposition technique.[25,27,28]

The optical, electrochemical, and spectro-electrochemical characteristics of the $TiO_2$@$WO_{3-x}$ and $TiO_2$/$WO_{3-x}$ mix thin films were measured and compared with those obtained with $TiO_2$ and $WO_{3-x}$.

Intrinsic oxygen vacancies improve the diffusion of $Li^+$ in the $WO_{3-x}$ NC host inducing a fast switching speed. Especially, the films obtained by using $TiO_2$@$WO_{3-x}$ heterostructures can switch from a fully transparent to a selective NIR blocking state and finally to a broad-band blocking state when the potential is further increased. A modulation of 89% between 300 and 1600 nm is reported. The practical application performance of $TiO_2$@$WO_{3-x}$ is thus corroborated with prototype dual-band EC devices fabricated on a highly transparent graphene substrate. Thanks to the higher NIR transparency of graphene than transparent conductive oxide films typically used (ITO, FTO, and AZO) in optoelectronic technologies, the device confirms the dual-band EC properties of the electrode, fast switching speed, and high coloration efficiency (CE) in both VIS and NIR regions. The electrical control of thermal radiation is expected to have an influence on several emerging technologies, including adaptive IR camouflage and heat management for space applications.

## 2. EXPERIMENTAL SECTION

**2.1. Synthesis of $WO_{3-x}$, $TiO_2$, and $TiO_2$@$WO_{3-x}$ NCs.** Water-dispersed sub-stoichiometric plasmonic inorganic $WO_{3-x}$ NCs were synthesized as reported elsewhere.[25] $TiO_2$ NCs were obtained following a previously reported procedure with some changes, mainly concerning the use of microwave irradiation as a heating source.[29] The overall synthetic strategy concerning the microwave synthesis of $TiO_2$ and $TiO_2$@$WO_{3-x}$-nanostructured materials will be published separately elsewhere.

**2.2. NC Airbrushing.** For the airbrushing deposition, the NC w/v solution was kept constant, as determined by thermogravimetric analysis. The $TiO_2$ and $WO_{3-x}$ composition within the NC blend was formulated starting from $TiO_2$ and $WO_{3-x}$ individual solutions based on the elemental (Ti and W) composition. Briefly, a 1:1 v/v water/ethanol NC solution (2.5 mg/mL) was deposited onto a 3 cm × 5 cm ITO glass substrate (or graphene substrate) using a Paasche airbrush operated with a 3.5 bar $N_2$ line gas. Before airbrushing, the ITO glass was treated with oxygen plasma (2 min, 50 W, 25 sccm, $1 \times 10^{-2}$ mbar). The NCs were deposited by holding the substrate at 100 °C on a laboratory heating plate and by using a Kapton mask to define the deposition area. The deposition was based on 150 short pulses of average 1 s each, using a 1 mm diameter tip nozzle held 15 cm from the substrate. An interval of 3 s between pulses was used to allow solvent evaporation. The NC-coated substrate was divided into several slides to perform the different characterizations. Afterward, thermal treatment at 300 °C for 30 min of the airbrushed samples was performed by using a hot plate to increase the nanocrystal-to-nanocrystal necking and remove Triton X-100. The thickness of the obtained airbrushed films was measured using a Veeco Dektak 150 + profiler.

**2.3. CVD-Graphene Growth and Transfer.** Graphene was grown on a 25 mm copper foil by the chemical vapor deposition (CVD) methodology at a temperature of 990 °C under a $H_2/CH_4$ (4/


https://doi.org/10.1021/acssuschemeng.3c00865
ACS Sustainable Chem. Eng. 2023, 11, 9601−9612

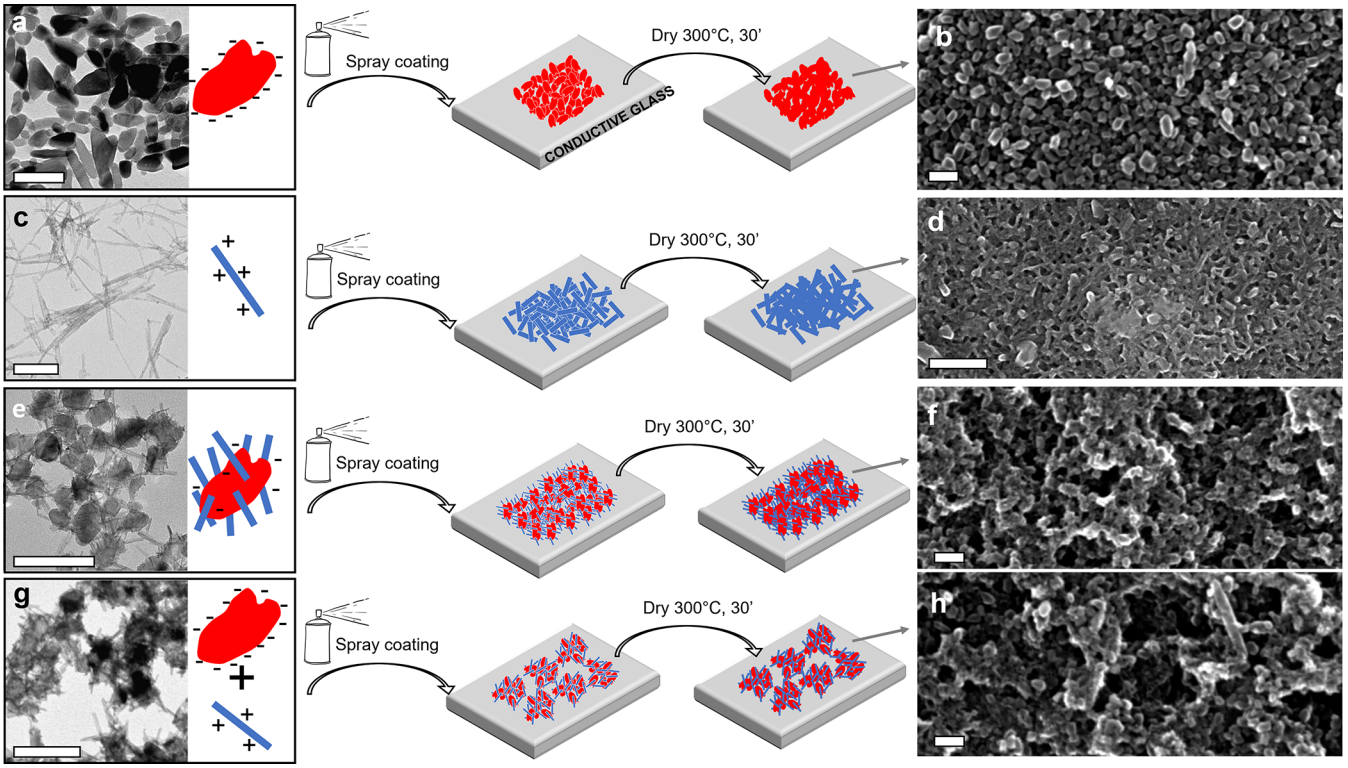


**Figure 1.** Schematic illustration of film-forming process obtained by the spray-coating technique followed by a thermal process (300 °C at 30 min). Representative low-resolution TEM images of as-synthesized nanostructures and corresponding SEM images of the deposited film for (a, b) $TiO_2$ NCs, (c, d) $WO_{3-x}$ NCs, (e, f) $TiO_2$@$WO_{3-x}$ heterostructures, and (g, h) the $TiO_2$/$WO_{3-x}$ blend. All scale bars are 100 nm.

1) gas flow. A thermal release tape procedure was employed to transfer the graphene layer to the Corning glass (ammonium persulfate solution was used as the copper etchant). A detailed description of the graphene growth and transfer process has been reported in ref 30.[30]

**2.4. Electron Microscopy Characterization.** Transmission and scanning electron microscopy (TEM and SEM) were used to perform topological and morphological measurements of sample solutions and films, respectively. Samples for low-resolution TEM analysis were obtained by transferring few drops of a dilute water-based solution onto standard carbon-coated Cu grids and waiting for the solvent to evaporate. After drying, the sample grids were kept overnight at 50 °C before imaging. TEM images of the sample grids were recorded on a Jeol JEM 1400 Plus microscope equipped with a $LaB_6$ filament source operating at 120 kV and a GATAN Orius SC600 CCD camera. SEM investigations were performed on samples spray-deposited onto ITO substrated, with FE-SEM Zeiss Merlin equipment equipped with a GEMINI2 column, Schottky-type electron gun and secondary electron/Inlens detectors. Images were recorded at 20kV.

**2.5. Electrochemical and Spectro-Electrochemical Characterization.** Electrochemical measurements of the films were performed in an electrolyte based on an anhydrous solution of 1 M $LiClO_4$ in propylene carbonate. A platinum foil was used as the counter electrode (area 4 $cm^2$), and an Ag/AgCl electrode (1 M $LiClO_4$ in propylene carbonate) was employed as the reference. All potentials are referred to as the Ag/AgCl reference electrode in 1 M $LiClO_4$ in propylene carbonate. The active area of the electrode was 1 $cm^2$. All measurements were made in the potential range of −0.8 to +1.0 V as determined via cyclic voltammetry (CV). Optical spectra were recorded at several potentials after allowing the optical signal to stabilize for 60 s. Chronopotentiometry was used to perform charge measurements between the potential limits, by switching the potential between −0.8 and +1.0 V for a holding time of 60 s. Stability tests were carried out via CV. All electrochemical measurements were performed using an AUTOLAB PGSTAT302N potentiostat and a Varian Cary 5000 UV−VIS−NIR spectrophotometer.

Integrated optical transmittance of the $TiO_2$@$WO_{3-x}$ NC film in the VIS region (380−780 nm) and NIR region (780−1600 nm) at −0.6 and −1.6 V is calculated considering the area between the transmittance at the open circuit potential and the selected curve.

Integrated solar irradiance transmittance of the $TiO_2$@$WO_{3-x}$ NC film in the VIS region ($T_{VIS}$, 380−780 nm), NIR region ($T_{NIR}$, 780−1600 nm), and total solar irradiation ($T_{sol}$, 350−1600 nm) is based on the following equation

$$T = \frac{\int T(\lambda)\psi(\lambda)\mathrm{d}\lambda}{\int \psi(\lambda)\mathrm{d}\lambda}$$

where $T(\lambda)$ is the transmittance at a wavelength of $\lambda$ and $\psi(\lambda)$ is the solar irradiance at 1.5 air mass.

## 3. RESULTS AND DISCUSSION

To evaluate the synergistic EC effect between $TiO_2$ and $WO_{3-x}$, nanostructured films were fabricated on ITO substrates with a controlled and uniform thickness through an optimized airbrush procedure. Figure 1 summarizes the overall deposition process involving four different batches of NCs. Figure 1a−d exhibits the reported representative low-resolution TEM images of $TiO_2$, $WO_{3-x}$, $TiO_2$@$WO_{3-x}$, and $TiO_2$/$WO_{3-x}$, respectively. $TiO_2$ NCs consist of nanostructures embedded in the anatase crystal lattice; $WO_{3-x}$ NCs are referred to as substoichiometric tungsten oxide nanorods with a $W_{18}O_{49}$ monoclinic crystal structure;[25] $TiO_2$@$WO_{3-x}$ is a nano-heterostructure whereby the $TiO_2$ anatase nanodomain enclosed in an octahedral shape is in lattice contact with a thin belt-shaped $WO_{3-x}$ structure that protrudes out or wraps around it; $TiO_2$/$WO_{3-x}$ indicates a mix of $TiO_2$ and $WO_{3-x}$ with a molar ratio comparable to the $TiO_2$@$WO_{3-x}$ heterostructure. All of the materials tested herein have been


https://doi.org/10.1021/acssuschemeng.3c00865
ACS Sustainable Chem. Eng. 2023, 11, 9601−9612

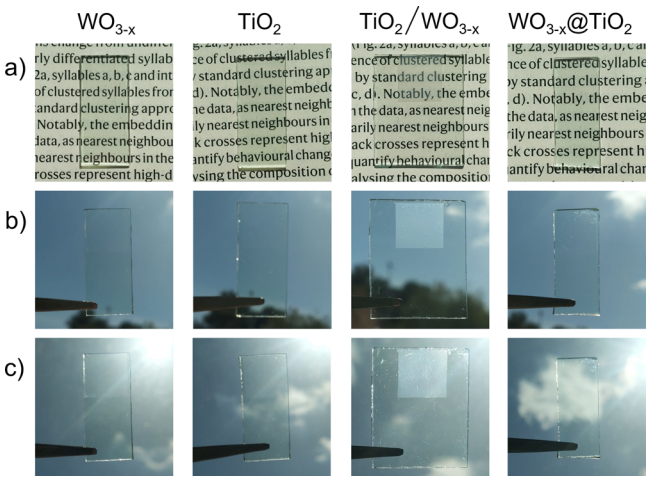


**Figure 2.** Images of $WO_{3-x}$ (column 1), $TiO_2$ (column 2), $TiO_2/WO_{3-x}$ (column 3) mix, and $TiO_2@WO_{3-x}$ (column 4) films airbrushed onto ITO substrates. The images have been acquired using different backgrounds: (a) newspaper, (b) sky light, and (c) sunshine in order to provide visual evidence of film transparency. The thickness of the films is 500 nm.

obtained within a hydroalcohothermal environment. The absence of organic long-alkyl chain passivating ligands during the NC growth process allows the use of a mild post-deposition treatment to render the NC surfaces available for further electrochemical reactions. The electrostatic repulsion of the charged surfaces ensures and guarantees colloidal stability in water over time. ζ-Potential measurements indicated that $TiO_2$ and $WO_{3-x}$ NCs possess opposite surface charges (−39 mV for $TiO_2$ nanocrystals and +2.87 mV for $WO_{3-x}$ NCs), and this feature was exploited to promote their interactions in the $TiO_2/WO_{3-x}$ mix. Therefore, the opposite charge of each colloid induces an electrostatic attractive force when they are mixed, resulting in a strong attraction between $WO_{3-x}$ and $TiO_2$.[31] On the other hand, this effect may favor the aggregation in the colloidal dispersion. To homogenize the drying kinetics, which influences the nanostructured electrode transparency, a hydroalcoholic combination of water/ethanol was used. Triton X-100 was both employed as a dispersing agent and used to modify the physical properties of the suspension in terms of increasing viscosity, reducing surface tension, and improving the adhesion of the particles to the ITO surface.[32,33] The nozzle-to-substrate distance was set at approximately 15 cm to avoid agglomeration of the particles. To prevent fractures and particle aggregation in the films, short spraying pulses were applied and the ITO substrate was placed onto a heating plate (100 °C) to accelerate the solvent evaporation. The atomic ratio between Ti and W atoms (calculated by ICP analysis, data not reported) was 2:1, both in the $TiO_2@WO_{3-x}$ and $TiO_2/WO_{3-x}$ blend samples. Afterward, thermal treatment of the airbrushed samples at 300 °C for 30 min was performed by using a hot plate to increase the NC-to-NC necking and remove Triton X-100. Optimization of the airbrush deposition process parameters enabled us to produce high-quality coatings.

SEM images of all of the films deposited onto ITO substrates are shown in Figure 1. A homogeneous surface is visible in all samples at the lowest magnification. $TiO_2$ samples show a granular morphology in which it is possible to observe that particles with a dimension of tens of nanometers are close to each other. A granular structure with a less-defined morphology is visible in SEM images of $TiO_2@WO_{3-x}$ and the $TiO_2/WO_{3-x}$ mix. Moreover, the thin film obtained with the $TiO_2/WO_{3-x}$ mix shows pores that are uniformly distributed over the entire surface of the film. A film with too high roughness can damage transparency. Indeed, high roughness and the presence of large pores and fractures act as light-trapping structures that reflect and disperse incident light. A moderate surface roughness value, on the other hand, enhances the capacity of the EC film to absorb the electrolyte, which improves EC performances. In this view, heterostructures exhibit the advantage of being based upon a lattice (and electrical) contact between both materials; in this case, the only possible factors of disorder arrangement are the interactions between single heterostructures unlike the blend for which several limits of interactions do exist, namely, between each single NC.

The optical characteristics of the annealed films were examined to investigate their transparency and haze. Haze is an optical effect caused by light scattering within a transparent material resulting in a cloudy or milky appearance, and it is obtained by the ratio between the diffuse and the total transmittance. Of course, in the field of EC devices, high transparency and low haze are desirable.

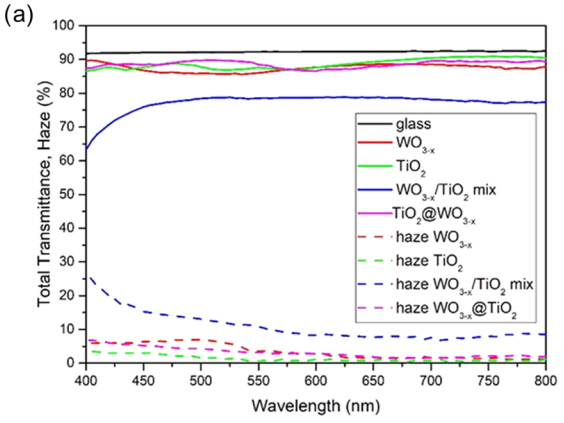


(b)

| Film | Average Transmittance |
|---|---|
| $WO_{3-x}$ | 88 % ± 2% |
| $TiO_2$ | 89 % ± 2% |
| $TiO_2/WO_{3-x}$ | 77 % ± 3% |
| $TiO_2@WO_{3-x}$ | 88 % ± 2% |

**Figure 3.** Transmittance spectra and investigated films' haze, as measured in relation to corrected air-baseline transmission on an ITO substrate: (a) (red) $WO_{3-x}$, (green) $TiO_2$, (blue) $WO_{3-x}$ /$TiO_2$ mix, and (purple) $TiO_2@WO_{3-x}$. The transmittance of glass (black) is also reported; (b) average transmittance of the films in the VIS light (400−800 nm).



https://doi.org/10.1021/acssuschemeng.3c00865
ACS Sustainable Chem. Eng. 2023, 11, 9601−9612

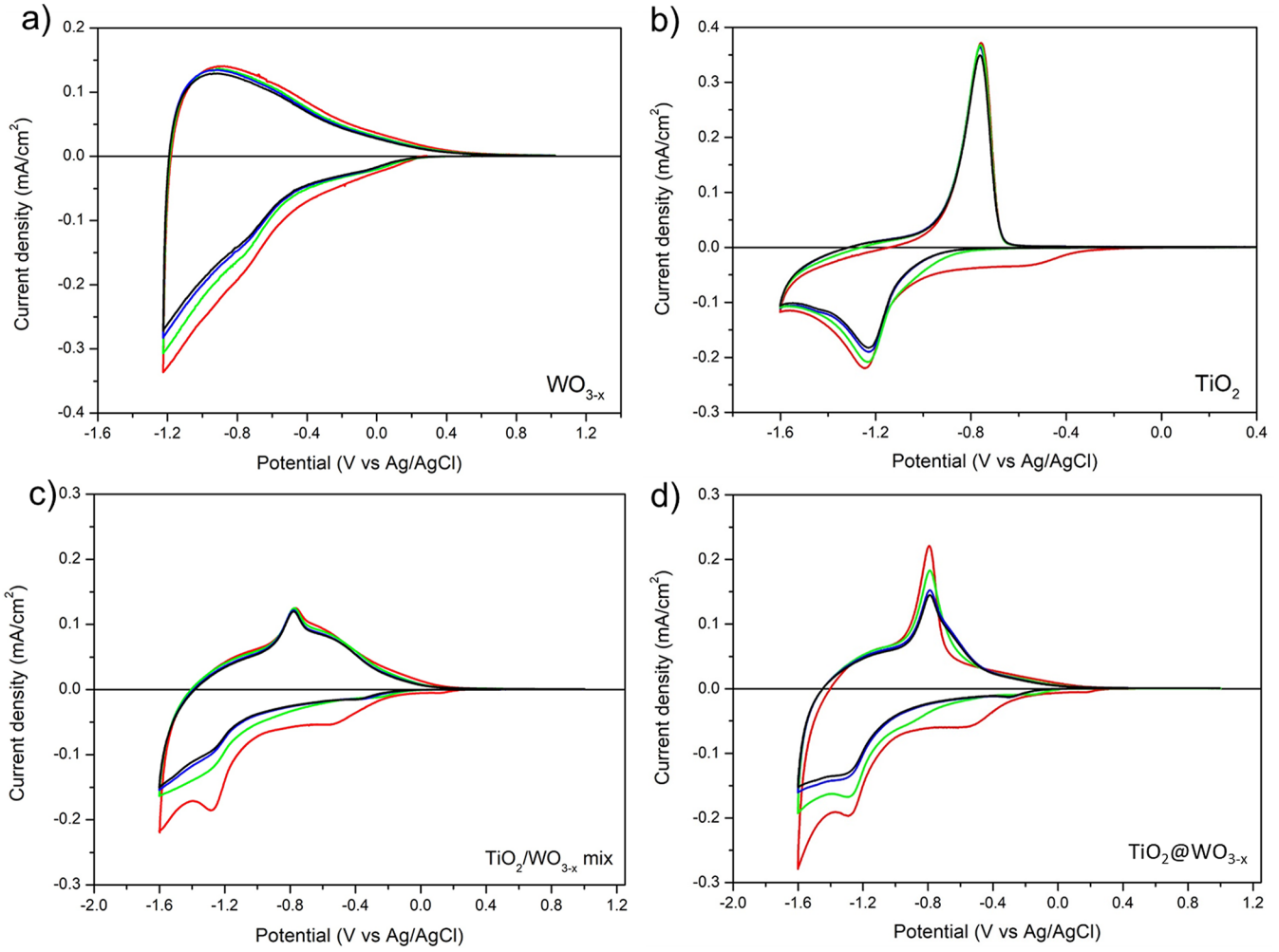


**Figure 4.** Cyclic voltammetry of investigated films taken in 1 M $LiClO_4$ in PC at a scan rate of 1 mV/s: (a) $WO_{3-x}$, (b) $TiO_2$, (c) $TiO_2/WO_{3-x}$ mix, and (d) $TiO_2@WO_{3-x}$.

Figure 2 shows images of $WO_{3-x}$, $TiO_2$, $TiO_2/WO_{3-x}$ mix, and $TiO_2@WO_{3-x}$ films airbrushed on ITO substrates, acquired using different backgrounds (newspaper, direct sky light, and sunshine). It is worth noting that all of the films, except for the $TiO_2/WO_{3-x}$ mix, have very high direct transmittance, with low light diffusion losses. Using newspaper or blue sky as background (Figure 2a,b), it is difficult to notice the presence of airbrushed films due to the very low haze, and it is necessary to increase the backlight, using sunshine as background (Figure 2c), to emphasize the light scattering and make the films visible. On the other hand, the sample with the $TiO_2/WO_{3-x}$ mix (Figure 2, column 3) shows a higher optical haze, which is imputable to the aggregation phenomena induced by the opposite charge of $WO_{3-x}$ and $TiO_2$ NCs.

With the aim at providing a quantitative measure of the optical performance of the films, in Figure 3 we exhibit the total transmittance and the haze of the four films, obtained by using an integrating sphere. From the reported spectra, it is evident that the obtained films are highly transparent in the VIS and NIR range of the electromagnetic spectrum. Moreover, the thin films show low optical haze with an average value lower than 8% for all samples in the 400−800 nm wavelength range. As expected, the higher haze value was measured for the sample based on the $TiO_2/WO_{3-x}$ mix (>10% in the full spectrum). Probably, the synthetic $TiO_2@WO_{3-x}$ heterostructures ensure a higher affinity between the components and a reduction of the scattering effects with respect to the $TiO_2/WO_{3-x}$ mix. Indeed, the previously reported SEM images suggest such an optical effect. Furthermore, as the film manufacturing process allows for the deposition of four films simultaneously, we determined the average transmittance (area below the transmittance spectrum) and calculated the relative error on the four films. The data are shown in Figure 3b. $WO_{3-x}$, $TiO_2$, and $TiO_2@WO_{3-x}$ films present a relative error of 2%. The maximum value of relative error is 3% for $TiO_2/WO_{3-x}$ mix films, probably related to the aggregation process during the deposition.

The four electrodes were subjected to CV measurements in the potential range of 1 to −1.6 V to ascertain their electrochemical characteristics. Figure 4 displays the first three voltammograms at a sweep rate of 2 mV/s. CV of the $WO_{3-x}$ thin film (Figure 3a) shows no noticeable peaks during the anodic scan. A peak is observed at −0.4 V, which can be attributed to the reduction process occurring in $WO_{3-x}$ during the intercalation of lithium ions.[34]

The $WO_{3-x}$ film, which served as the anode in a lithium-ion battery, was the topic of earlier studies that showed cyclic voltammograms with two or three strong peaks in the first cycle. These peaks were either related to an electrochemical reaction between lithium ions and $WO_{3-x}$ or to the formation


https://doi.org/10.1021/acssuschemeng.3c00865
ACS Sustainable Chem. Eng. 2023, 11, 9601−9612

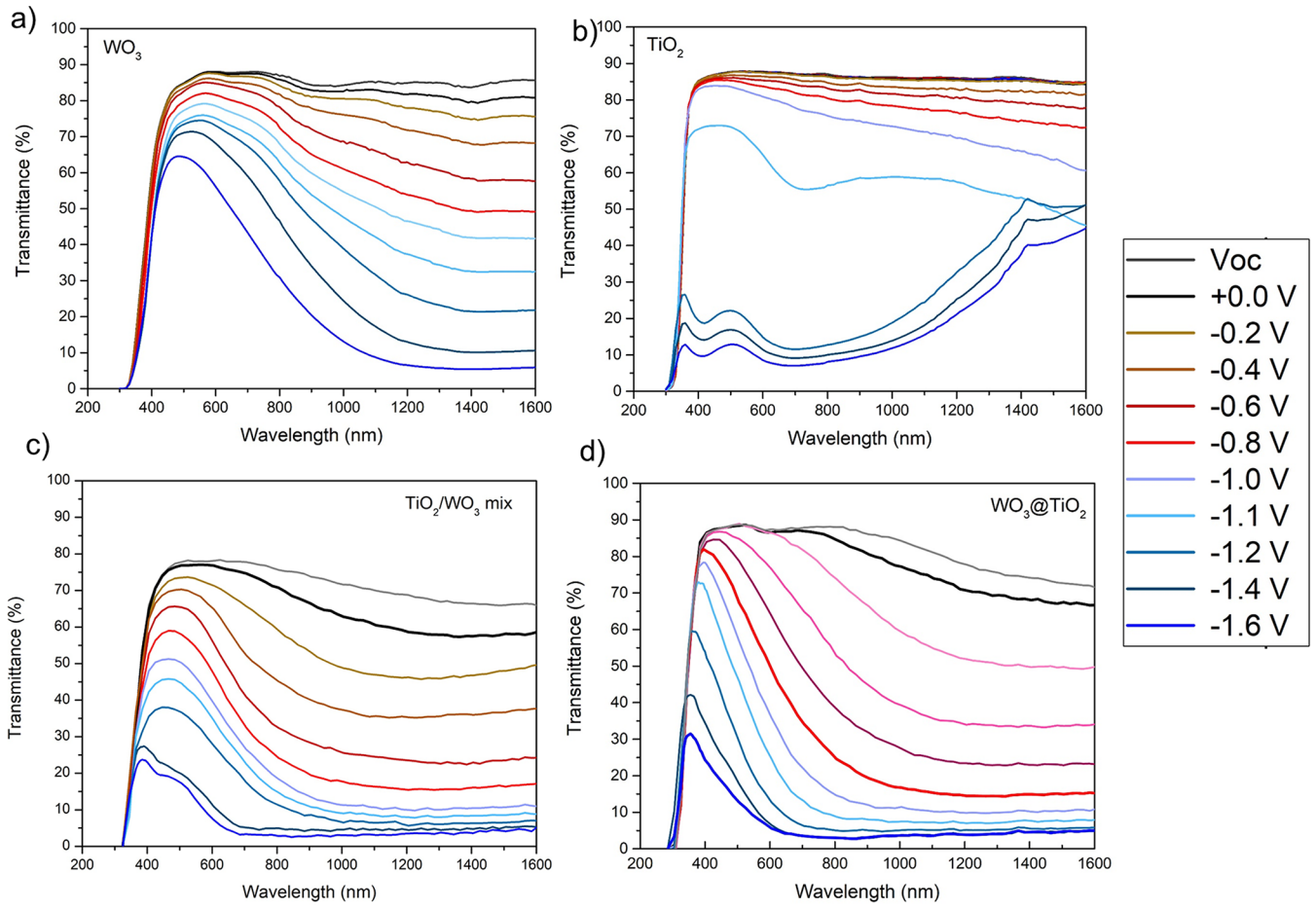


**Figure 5.** Spectro-electrochemical characterization of investigated films in 1 M $LiClO_4$ in PC: (a) $WO_{3-x}$, (b) $TiO_2$, (c) $TiO_2/WO_{3-x}$ mix, and (d) $TiO_2@WO_{3-x}$.

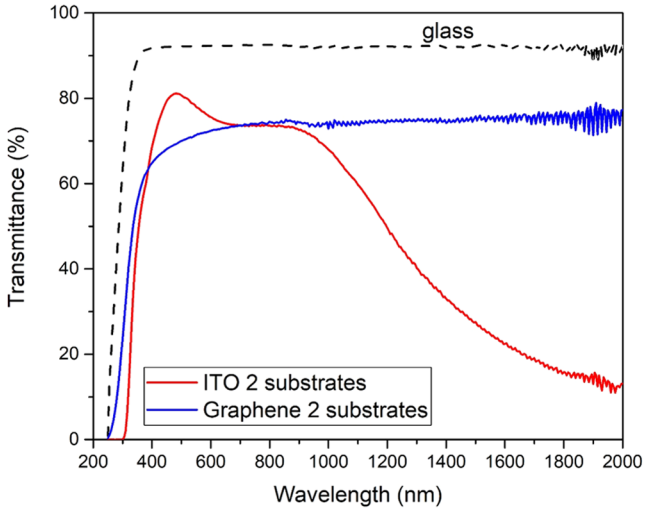


**Figure 6.** Transmittance spectra of ITO and graphene substrates.

of an interphase layer based on a thick solid electrolyte on the electrode surface.[35,36] The absence of peaks or the presence of weak peaks in the CV scan in our case is probably due to the fact that severe structural changes are sufficiently suppressed by the mesoporous structure of the belt-shaped $WO_{3-x}$ NC electrode.[37,38] A small irreversible capacity loss is evident in the first CV cycle and is imputable to the phase change or ion trapping events at the defect sites of the $WO_{3-x}$ electrode.[36,37]

Figure 4b shows the cyclic voltammogram of $TiO_2$. A cathodic peak is observed at around −1.2 V, and the corresponding anodic peak is seen at around −0.80 V. These peaks are related to the reduction reaction of $Ti^{4+}$ to $Ti^{3+}$ and the subsequent re-oxidation to $Ti^{4+}$. As shown in Figure 4c,d, $TiO_2/WO_{3-x}$- and $TiO_2@WO_{3-x}$-based films have a similar voltammogram. Both exhibit the combined electrochemical properties of $WO_{3-x}$ and $TiO_2$. In particular, the two voltammograms present a small cathodic peak at −0.4 V ascribable to the reduction of $WO_{3-x}$ and reduction/oxidation peaks of $TiO_2$ at −1.2 and −0.8 V. Moreover, the two voltammograms show the same onset potential of the charge accumulation located at about −0.2 V. Afterward, the four nanostructured electrodes were studied spectro-electrochemically to investigate their performance as an active EC coating (Figure 5).

The application of a low electric field leads to the intercalation/deintercalation of $Li^+$ together with charge-balancing electrons, resulting in an optical modulation from a bleached to a colored state and back.[39−41] Low intercalation levels of $Li^+$ species (with $Li^+/W$ ratio ($x$) of about 0.05) in the crystalline tungsten oxide (Figure 5a) result in the creation of intermediate polaronic states at an energy below that of the conduction band (CB).[42] At higher intercalation ratios ($0.05 < x < 0.15$), an overlapping and merging of the polaronic states with the CB is induced, and at even higher values of $x$, the inserted electrons begin to occupy the bottom portion of the CB.[41,42] Electrons in extended delocalized states behave like



https://doi.org/10.1021/acssuschemeng.3c00865
ACS Sustainable Chem. Eng. 2023, 11, 9601−9612

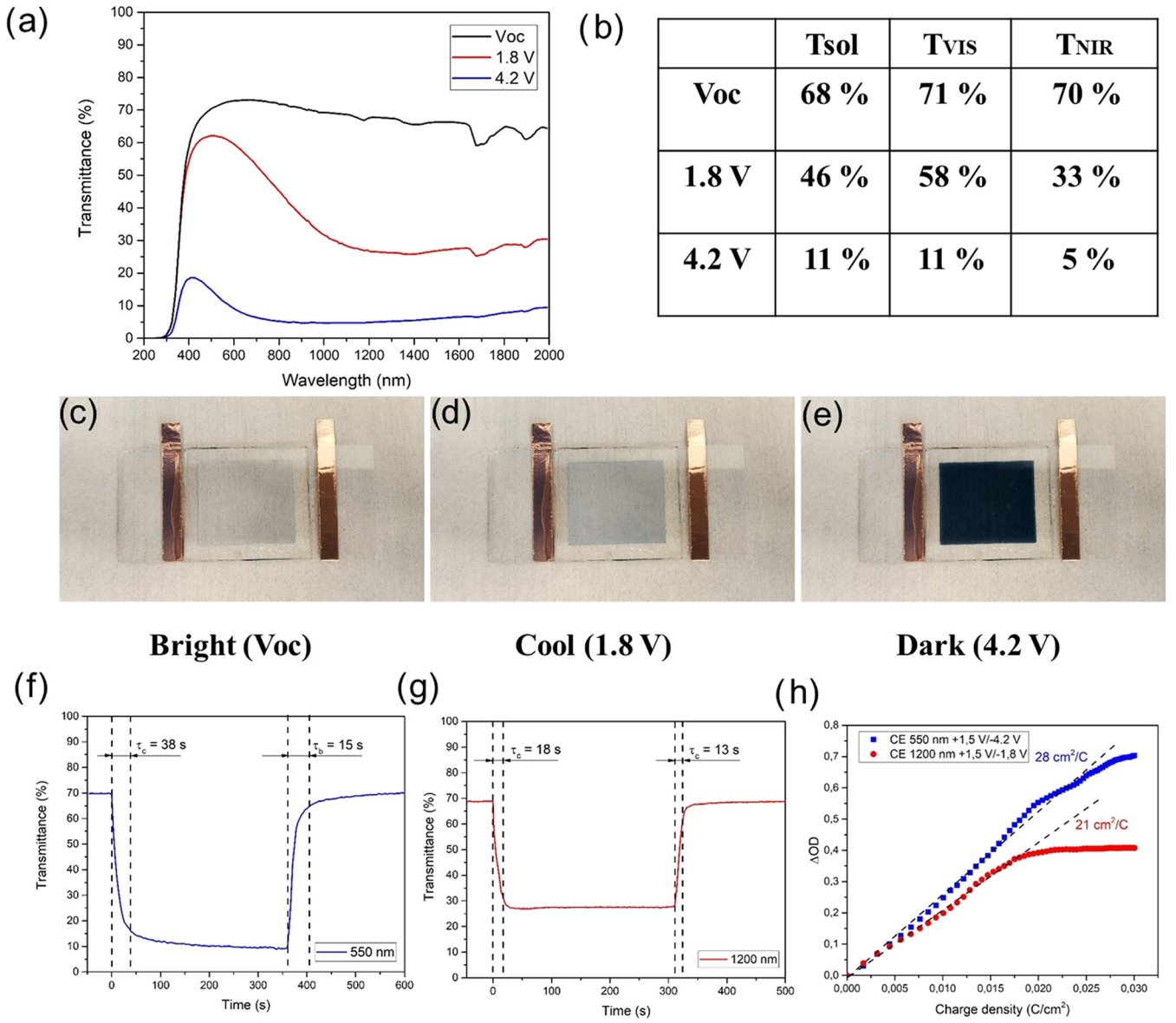


| | Tsol | Tvis | Tnir |
|---|---|---|---|
| Voc | 68 % | 71 % | 70 % |
| 1.8 V | 46 % | 58 % | 33 % |
| 4.2 V | 11 % | 11 % | 5 % |

**Figure 7.** EC performance of the $TiO_2$@$WO_{3-x}$-based device. (a) Optical transmittance spectra band, (b) integrated solar irradiance transmittance of the device in the VIS light (380−780 nm), NIR region (780−1900 nm), and total solar irradiation (sol, 380−2200 nm) at $V_{oc}$, 1.8, and 4.2 V. (c, d, e) Corresponding digital photos. In situ optical responses (f) at 550 nm in the $V_{oc}$/−4.2 V potential window and (g) at 1200 nm in the $V_{oc}$/−1.8 V potential window. (h) Plot of optical density variation as a function of charge density monitored at 550 nm (blue dots) and 1600 nm (red dots), respectively.

free electrons; thus, Drude-type absorption models can be used to describe reflective optical modulation.[43]

Crystalline $WO_{3-x}$ ($cWO_{3-x}$) is an insulator for $x < 0.1$, while it undergoes an Anderson transition and exhibits metallic behavior for $x > 0.1$.[43] Therefore, in the insulating phase, only polaron hopping is observed, whereas in metallic compositions, the optical absorption in $cWO_{3-x}$ is due to the coexistence of polaron-based and Drude-type free electrons.[43] Figure 5b shows the transmittance of a mesoporous $TiO_2$ film. Upon the application of different bias voltages, the electrodes change color from transparent to dark blue when lithium is inserted.[44−46]

The EC effect is due to the electrons that enter the material with Li ions to maintain the charge balance, and a variety of mechanisms have been proposed for the origin of the EC effect in Li-inserted $TiO_2$: photon adsorption by free electrons, localized electrons, polaron absorption due to localization of electrons on $Ti^{3+}$ ions, and trapping of electrons in surface states.[47−49] Between 0.2 and −1.0 V, a double layer is formed at the electrode/electrolyte interface (see CV) with, on the one hand, electrons in the space-charge region within $TiO_2$ and, on the other hand, the adsorption of charged species from the electrolyte. As a consequence, a monotonic wavelength rise is seen, which strikingly resembles delocalized electron absorption.[47] An absorbance reduction at about 350 nm, near the band gap, supports this. This so-called Burstein−Moss shift, which is well known for $TiO_2$ in the double-layer regime, is brought on by (nearly)-free electrons populating the bottom of the CB. The absorption caused by free electrons increases as additional electrons are introduced. The $TiO_2$ film is transparent to the naked eye down to −1.0 V, and the total absorption in the double-layer regime is relatively low. The


https://doi.org/10.1021/acssuschemeng.3c00865
ACS Sustainable Chem. Eng. 2023, 11, 9601−9612

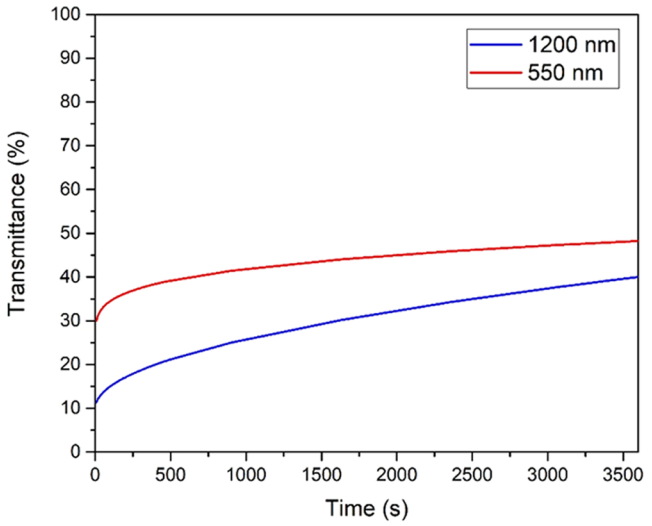


**Figure 8.** Optical memory of the $TiO_2$@$WO_{3-x}$-based device monitored at 1200 and 550 nm, respectively, recorded after charging the device at 4.2 V for 300 s and keeping it for 1 h in open-circuit conditions.

charge compensation mechanism alters at a potential of roughly −1.20 V, just before the phase transition begins. Lithium-ion intercalation, which provides local charge adjustment, now occurs in conjunction with electron injection. It is obvious that intercalation causes the absorbance to significantly rise and the structure of the spectrum to significantly shift. At around 410 and 700 nm, two large absorption peaks are observed. Inferring that the dark hue of $Li_{0.5}TiO_2$ is not due to (almost) free electrons but localized electrons, it is suggested that electrons in $Li_{0.5}TiO_2$ are less free than those in $TiO_2$ in the double-layer region. The decrease in absorption in the infrared region is consistent with this.

Regarding the mixed materials (Figure 5c,d), $TiO_2$/$WO_{3-x}$ mix and $TiO_2$@$WO_{3-x}$ heterostructures, both show similar spectro-electrochemical behavior with the applied voltage. In particular, independent control of the VIS and NIR regions of the electromagnetic spectrum can be achieved by regulating the applied voltage. Taking into account the behavior of the $TiO_2$@$WO_{3-x}$ electrode, the film is completely transparent in the VIS and NIR range when the applied voltage is higher than or equal to −0.4 V. Such an operation regime is defined as a "bright" mode, and it is desirable for high visibility and indoor heating thanks to the passage of infrared radiation. When the applied potential is reduced to −0.6 V, the material is in the "cool" mode and the film can block 67% of the NIR radiation and remains transparent in the VIS range, with more than 60% of average transmittance. Such a performance mode is ideal during summer when the indoor heating effect due to infrared irradiation should be minimized. In such conditions, the selective NIR modulation is attributable to free electron absorption of $WO_{3-x}$ (Drude-type absorption). When the potential is further reduced, lithium ions intercalate into the thin film inducing a phase transformation of the material and a

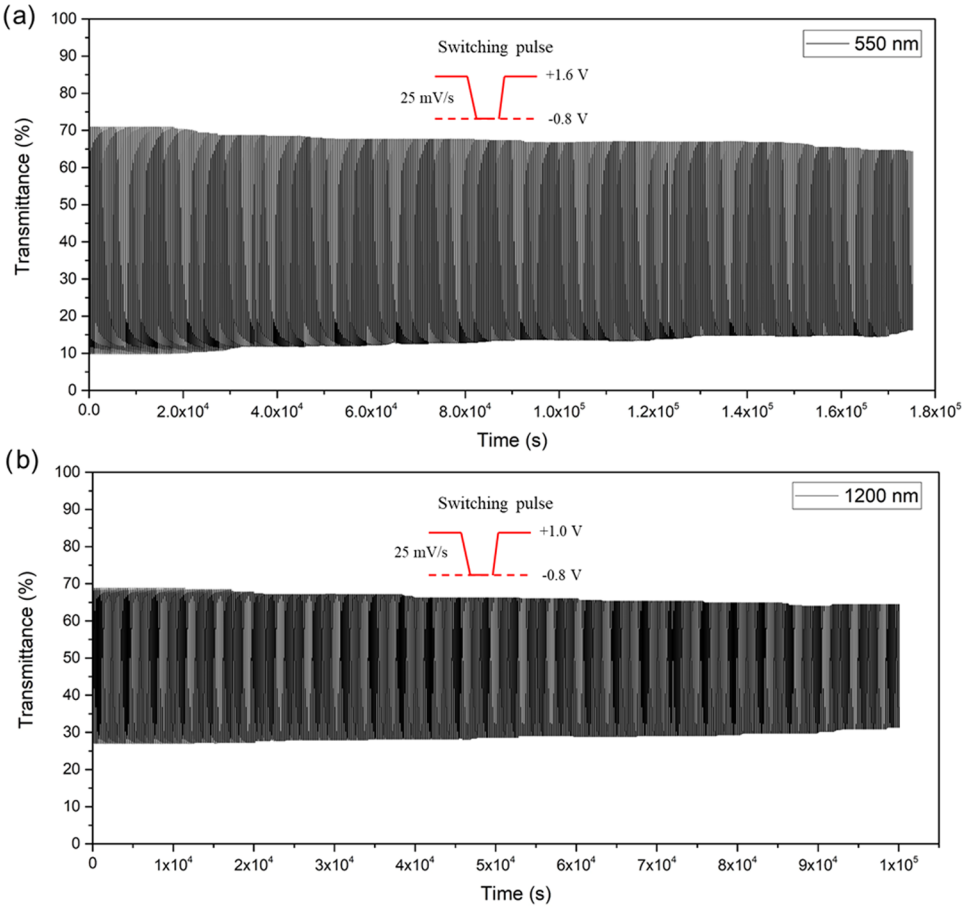


**Figure 9.** Stability test of $TiO_2$@$WO_{3-x}$-based device monitored in situ at (a) 550 nm and (b) 1200 nm.



https://doi.org/10.1021/acssuschemeng.3c00865
ACS Sustainable Chem. Eng. 2023, 11, 9601−9612

modulation of the visible light, until a "dark" mode is reached at −1.6 V (VIS 83%, NIR 76%).

Considering the characterization of the reported thin films, the main difference between the two films (blend versus heterostructure) lies in the lower ability of the $TiO_2/WO_{3-x}$ mix-based film to modulate the VIS part of the solar spectrum due to the high haze of the film. As a consequence, the $TiO_2@WO_{3-x}$ film represents the best compromise in terms of good thin film morphology, low optical haze, and good dual-band EC modulation. In order to get further insight into the EC properties of the $TiO_2@WO_{3-x}$ film, coloration/bleaching kinetics, CE, and stability tests were carried out (Figure S1). Switching kinetics were measured by monitoring in situ the optical transmittance variation at 550 and 1200 nm, with the potential switched between −1.6 and +0.7 V for a 100 s holding time. A coloration time $\tau_c$ (defined as the time to reach a 90% of the maximum $\Delta T$) of 22 and 5 s was recorded at 550 and 1200 nm, respectively. This difference is related to the lower amount of charge needed to modulate the transmittance at 1200 nm. However, the bleaching process at 550 nm is faster than that at 1200 nm, requiring 4 and 22 s, respectively. This can be correlated to a higher driving force (applied voltage) applied to the film.

CE is one of the most helpful metrics for assessing the quality of an EC product or device. Large optical modulation with less charge insertion is produced by a high CE. At 550 and 1200 nm, respectively, the CE was estimated from the slope of the linear section of the optical density as a function of the charge density (Figure S1c). For conventional EC materials that experience ion intercalation, such as $WO_3$, typical values of CE at 600 nm wavelength range from 50 to 60 $cm^2/C$.[39] Since the use of a lower insertion or extraction charge increases long-term cycle stability, high CE can give significant optical modulation with minimal variations in insertion or extraction amounts, making it an important feature for practical devices. CV was used to examine the stability of the $TiO_2@WO_{3-x}$ film by testing the device to 500 coloring/bleaching cycles. The film was cycled between −1.6 and +1.0 V with a scan rate of 2 mV/s (Figure S2a). The discharge current (positive current) was lowered by roughly 11% after 500 cycles, but the charging current (negative current) appeared to have been unaffected. The result was a 5% decrease in transmittance over the whole wavelength range in the bleached (and colored) conditions (Figure S2b). The $TiO_2@WO_{3-x}$ film did not show any macroscopic cracks or obvious evidence of deterioration following the stability test.

To exploit the dual-band electrochromism of the $TiO_2@WO_{3-x}$ thin film, it was deposited on graphene-coated glass substrates to fabricate an EC device.

The graphene substrate exhibits high transparency in the VIS light spectrum, which is comparable to ITO, while the transmittance in the NIR region exceeded that of ITO which has strong absorption over 1100 nm. However, although a reduction in transmittance is visible when two graphene/glass substrates are employed (anode and cathode), there is still a high transmittance in the NIR region, unlike what has been measured for two ITO/glass substrates (see Figures 6 and S3). In particular, the transmittance spectra exhibited in Figure 6 are related to glass substrates with two layers of graphene, with a sheet resistance of ≈250 $\Omega \cdot sq^{-1}$, which is in line with the $R_s$ values of multilayer graphene reported in ref 30.[30]

A prototype of the EC device was assembled by using two graphene/glass substrates and $TiO_2@WO_{3-x}$. In the obtained device, the $TiO_2@WO_{3-x}$ deposited on top of a graphene/glass substrate is the cathodic part, the anode is constituted by a graphene/glass coated with $SnO_2$, and a 1 M solution of $LiClO_4$ in propylene carbonate dissolved in acetovinylic-based gel is employed as the electrolyte.[50]

The device exhibits a dual-band modulation as reported in the characterization of the single thin film in the three-electrode configuration. The transmittance modulation of the device at 550 and 1200 nm in the three modes (bright, cool, and dark) is reported in the table appearing in Figure 7b and the related spectra are reported in Figure 7a. To the best of our knowledge, this is the first time that a dual-band EC device was fabricated by employing NIR transparent electrodes. The images of the device in the "bright", "cool", and "dark" modes are also exhibited (Figure 7c−e). Moreover, the solar irradiance spectra of the $WO_{3-x}@TiO_2$-based device in the "bright", "cool", and "dark" states are shown in Figure 7b. Such spectra are calculated considering the solar energy distribution at different wavelengths of the electromagnetic spectrum; therefore, they provide more accurate information about the performances of the reported thin film for the modulation of solar irradiation. According to such spectra, the film can block 67% of solar heat in the NIR range when it is in the "cool" state (1.8 V), preserving an excellent transmittance in the VIS region (64%) to ensure good daylighting (Figure 7b). Such operation mode provides a remarkable reduction of the building energy costs due to air-conditioning and lighting. At 4.2 V, when the sample is in the "dark" mode, 89% of VIS light and 89% of solar heat are blocked, which is an ideal condition for further reducing solar heat gain in buildings and ensuring personal privacy.

Kinetics is another important characteristic that should be evaluated for EC devices. The switching time of the $TiO_2@WO_{3-x}$ film-based EC device from the "bright" to the "dark" mode at 550 and 1200 nm is reported in Figure 7f,g. The coloration time ($\tau c$) at 550 nm equals 38 s, while the bleaching time ($\tau b$) is 15 s. The $\tau c$ and the $\tau b$ at 1200 nm are 18 and 13 s, respectively. CE in the VIS (550 nm) and NIR (1200 nm) regions was also calculated and the results are displayed in Figure 7h.

Figure 8 shows the memory effect recorded by in situ monitoring of the transmittance at 550 and 1200 nm, respectively, after the device was powered for 300 s under coloring conditions (4.2 V) and kept in open-circuit conditions for 1 h. The $TiO_2@WO_{3-x}$-based device preserves part of its color, increasing its transmittance in the VIS light (550 nm) from 10 to 40% and in the NIR (1200 nm) from 30 to 45%. Such a high optical stability is beneficial for an EC device as it eliminates the need for a constant voltage to maintain the color of the device.

In order to assess the stability of the $TiO_2@WO_{3-x}$-based device, 500 coloring/bleaching cycles were carried out by monitoring the transmittance at 550 and 1200 nm. Coloration/bleaching kinetics were measured with the potential switched between −1.6/+1.0 V and −0.8/+1.0 V at 550 and 1200 nm, respectively. A scan rate of 25 mV/s was used to reach the coloring and bleaching potentials. Analysis of the plots shown in Figure 9 reveals that the modulation of transmittance decreases from 60 to 47% at 550 nm and from 40 to 33% at 1200 nm. After the stability test, the $TiO_2@WO_{3-x}$ device did not show any signs of degradation or the presence of blisters in the gel electrolyte.



https://doi.org/10.1021/acssuschemeng.3c00865
ACS Sustainable Chem. Eng. 2023, 11, 9601−9612

## 4. CONCLUSIONS

We presented a proof of concept of an innovative dual-band EC device able to selectively and independently modulate the VIS and NIR range of the electromagnetic spectrum, thus operating in "bright", "cool", and "dark" modes. The selective dual-band operative conditions were achieved by using the cooperative spectro-electrochemical properties of $WO_{3-x}$ and $TiO_2$ either deposited as pre-synthesized $TiO_2@WO_{3-x}$ nano-heterostructures or out from a simply blended mixture of individual colloidal solutions. However, the solution-processable $TiO_2@WO_{3-x-x}$ heterostructure represented a better candidate for the fabrication of an EC device due to an improved homogeneity and morphology of the thin film and excellent optical properties in terms of transparency and low haze.

Considering the interesting EC properties of the obtained thin film, a full device was fabricated for the first time by using graphene as an NIR transparent electrode which, differently from common conductive electrodes (such as ITO, which is an NIR absorbing material), allows a real light modulation in the NIR region, since it preserves a great transmittance in that wavelength range.

Our results suggest that the $TiO_2@WO_{3-x}$ heterostructure deposited on a graphene substrate represents a valid candidate for the future development of large-scale dual-band EC devices because of the combination of unquestioned advantages spanning from NC sample scalability due to the valuable synthetic procedure (MW-assisted synthesis), large-area deposition method (spray-coating airbrushing technique), and mild conditions of sample heating treatments aimed at thin film manufacturing (300 °C).

## ■ ASSOCIATED CONTENT

### Supporting Information

The Supporting Information is available free of charge at https://pubs.acs.org/doi/10.1021/acssuschemeng.3c00865.

> Electrochemical characterization of the TiO2@$WO_{3-x}$ electrode in a 3-electrode setup; stability test of the TiO2@$WO_{3-x}$ electrode in a 3-electrode setup; transmittance spectra of ITO and graphene substrates (PDF)

## ■ AUTHOR INFORMATION


### Corresponding Authors

**Roberto Giannuzzi** − *CNR-NANOTEC—Institute of Nanotechnology, 73100 Lecce, Italy; Department of Mathematics and Physics, University of Salento, 73100 Lecce, Italy;* orcid.org/0000-0002-0997-5686; Email: roberto.giannuzzi@nanotec.cnr.it

**Luigi Carbone** − *CNR-NANOTEC—Institute of Nanotechnology, 73100 Lecce, Italy;* orcid.org/0000-0002-1369-6890; Email: luigi.carbone@nanotec.cnr.it

### Authors

**Marco Pugliese** − *CNR-NANOTEC—Institute of Nanotechnology, 73100 Lecce, Italy*

**Riccardo Scarfiello** − *CNR-NANOTEC—Institute of Nanotechnology, 73100 Lecce, Italy*

**Carmela Tania Prontera** − *CNR-NANOTEC—Institute of Nanotechnology, 73100 Lecce, Italy;* orcid.org/0000-0002-5934-7733

**Giuseppe Valerio Bianco** − *Department of Chemistry, Apulian Graphene Lab, CNR-NANOTEC—Institute of Nanotechnology, University of Bari, Bari 70126, Italy*

**Giovanni Bruno** − *Department of Chemistry, Apulian Graphene Lab, CNR-NANOTEC—Institute of Nanotechnology, University of Bari, Bari 70126, Italy*

**Sonia Carallo** − *CNR-NANOTEC—Institute of Nanotechnology, 73100 Lecce, Italy*

**Fabrizio Mariano** − *CNR-NANOTEC—Institute of Nanotechnology, 73100 Lecce, Italy*

**Antonio Maggiore** − *CNR-NANOTEC—Institute of Nanotechnology, 73100 Lecce, Italy*

**Giuseppe Gigli** − *CNR-NANOTEC—Institute of Nanotechnology, 73100 Lecce, Italy*

**Vincenzo Maiorano** − *CNR-NANOTEC—Institute of Nanotechnology, 73100 Lecce, Italy*

Complete contact information is available at: https://pubs.acs.org/10.1021/acssuschemeng.3c00865

### Author Contributions

‖M.P. and R.S. contributed equally to this work.


### Notes

The authors declare no competing financial interest.

## ■ ACKNOWLEDGMENTS

This work was supported by "ECO-sustainable and intelligent fibers and fabrics for TEChnic clothing (ECOTEC)", PON ≪R&I≫ 2014−2020, project No. ARS01_00951, CUP B66C18000300005; Progetto FISR—C.N.R. "Tecnopolo di nanotecnologia e fotonica per la medicina di precisione"—CUP B83B17000010001. PE4 PNRR MUR project PE0000023−NQSTI; PNRR MUR project IR0000016−I−PHOQS; the Italian Ministry of Research (MUR) under the complementary actions to the NRRP (PNC0000007) "Fit4MedRob- Fit for Medical Robotics" Grant (contract number CUP B53C22006960001). RG acknowledges Regione Puglia and ARTI for founding FIR—Future in Research projects no. UNISAL034. All Authors acknowledge the open access CNR staff for support in open access publishing.

## ■ REFERENCES

(1) Pérez-Lombard, L.; Ortiz, J.; Pout, C. A Review on Buildings Energy Consumption Information. *Energy Build.* **2008**, *40*, 394−398.

(2) Gago, E. J.; Muneer, T.; Knez, M.; Köster, H. Natural Light Controls and Guides in Buildings. Energy Saving for Electrical Lighting, Reduction of Cooling Load. *Renewable Sustainable Energy Rev.* **2015**, *41*, 1−13.

(3) Werner, S. International Review of District Heating and Cooling. *Energy* **2017**, *137*, 617−631.

(4) Cuce, E.; Riffat, S. B. A State-of-the-Art Review on Innovative Glazing Technologies. *Renewable Sustainable Energy Rev.* **2015**, *41*, 695−714.

(5) Hee, W. J.; Alghoul, M. A.; Bakhtyar, B.; Elayeb, O.; Shameri, M. A.; Alrubaih, M. S.; Sopian, K. The Role of Window Glazing on Daylighting and Energy Saving in Buildings. *Renewable Sustainable Energy Rev.* **2015**, *42*, 323−343.

(6) Cannavale, A.; Ayr, U.; Fiorito, F.; Martellotta, F. Smart Electrochromic Windows to Enhance Building Energy Efficiency and Visual Comfort. *Energies* **2020**, *13*, No. 1449.

(7) Wu, M.; Shi, Y.; Li, R.; Wang, P. Spectrally Selective Smart Window with High Near-Infrared Light Shielding and Controllable Visible Light Transmittance. *ACS Appl. Mater. Interfaces* **2018**, *10*, 39819−39827.

(8) Cai, G.; Eh, A. L.-S.; Ji, L.; Lee, P. S. Recent Advances in Electrochromic Smart Fenestration. *Adv. Sustainable Syst.* **2017**, *1*, No. 1700074.
(9) Giannuzzi, R.; De Donato, F.; De Trizio, L.; Monteduro, A. G.; Maruccio, G.; Scarfiello, R.; Qualtieri, A.; Manna, L. Tunable Near-Infrared Localized Surface Plasmon Resonance of F, In-Codoped CdO Nanocrystals. *ACS Appl. Mater. Interfaces* **2019**, *11*, 39921−39929.
(10) Runnerstrom, E. L.; Llordés, A.; Lounis, S. D.; Milliron, D. J. Nanostructured Electrochromic Smart Windows: Traditional Materials and NIR-Selective Plasmonic Nanocrystals. *Chem. Commun.* **2014**, *50*, 10555−10572.
(11) Williams, T. E.; Chang, C. M.; Rosen, E. L.; Garcia, G.; Runnerstrom, E. L.; Williams, B. L.; Koo, B.; Buonsanti, R.; Milliron, D. J.; Helms, B. A. NIR-Selective Electrochromic Heteromaterial Frameworks: A Platform to Understand Mesoscale Transport Phenomena in Solid-State Electrochemical Devices. *J. Mater. Chem. C* **2014**, *2*, 3328−3335.
(12) Runnerstrom, E. L.; Bergerud, A.; Agrawal, A.; Johns, R. W.; Dahlman, C. J.; Singh, A.; Selbach, S. M.; Milliron, D. J. Defect Engineering in Plasmonic Metal Oxide Nanocrystals. *Nano Lett.* **2016**, *16*, 3390−3398.
(13) Wang, K.; Meng, Q.; Wang, Q.; Zhang, W.; Guo, J.; Cao, S.; Elezzabi, A. Y.; Yu, W. W.; Liu, L.; Li, H. Advances in Energy-Efficient Plasmonic Electrochromic Smart Windows Based on Metal Oxide Nanocrystals. *Adv. Energy Sustainability Res.* **2021**, *2*, No. 2100117.
(14) Zhang, W.; Li, H.; Hopmann, E.; Elezzabi, A. Y. Nanostructured Inorganic Electrochromic Materials for Light Applications. *Nanophotonics* **2021**, *10*, 825−850.
(15) Kriegel, I.; Scotognella, F.; Manna, L. Plasmonic Doped Semiconductor Nanocrystals: Properties, Fabrication, Applications and Perspectives. *Phys. Rep.* **2017**, *674*, 1−52.
(16) Lounis, S. D.; Runnerstrom, E. L.; Llordés, A.; Milliron, D. J. Defect Chemistry and Plasmon Physics of Colloidal Metal Oxide Nanocrystals. *J. Phys. Chem. Lett.* **2014**, *5*, 1564−1574.
(17) Barawi, M.; De Trizio, L.; Giannuzzi, R.; Veramonti, G.; Manna, L.; Manca, M. Dual Band Electrochromic Devices Based on Nb-Doped TiO2 Nanocrystalline Electrodes. *ACS Nano* **2017**, *11*, 3576−3584.
(18) Cao, S.; Zhang, S.; Zhang, T.; Lee, J. Y. Fluoride-Assisted Synthesis of Plasmonic Colloidal Ta-Doped TiO2 Nanocrystals for Near-Infrared and Visible-Light Selective Electrochromic Modulation. *Chem. Mater.* **2018**, *30*, 4838−4846.
(19) Cao, S.; Zhang, S.; Zhang, T.; Yao, Q.; Lee, J. Y. A Visible Light-Near-Infrared Dual-Band Smart Window with Internal Energy Storage. *Joule* **2019**, *3*, 1152−1162.
(20) Park, S.; Park, H. S.; Dao, T. T.; Song, S. H.; Lee, S. I.; Van Tran, H.; Ullah, A.; Han, C.-H.; Hong, S. Solvothermal Synthesis of Oxygen Deficient Tungsten Oxide Nano-Particle for Dual Band Electrochromic Devices. *Sol. Energy Mater. Sol. Cells* **2022**, *242*, No. 111759.
(21) Zhang, S.; Cao, S.; Zhang, T.; Lee, J. Y. Plasmonic Oxygen-Deficient TiO2-x Nanocrystals for Dual-Band Electrochromic Smart Windows with Efficient Energy Recycling. *Adv. Mater.* **2020**, *32*, No. 2004686.
(22) Llordés, A.; Garcia, G.; Gazquez, J.; Milliron, D. J. Tunable Near-Infrared and Visible-Light Transmittance in Nanocrystal-in-Glass Composites. *Nature* **2013**, *500*, 323−326.
(23) Dong, A.; Ye, X.; Chen, J.; Kang, Y.; Gordon, T.; Kikkawa, J. M.; Murray, C. B. A Generalized Ligand-Exchange Strategy Enabling Sequential Surface Functionalization of Colloidal Nanocrystals. *J. Am. Chem. Soc.* **2011**, *133*, 998−1006.
(24) Lakhanpal, V. S.; Zydlewski, B. Z.; Gan, X. Y.; Celio, H.; Jhong, H.-R. "Molly".; Ofosu, C. K.; Milliron, D. J. Aqueous Transfer of Colloidal Metal Oxide Nanocrystals via Base-Driven Ligand Exchange. *Chem. Commun.* **2022**, *58*, 9496−9499.
(25) Scarfiello, R.; Prontera, C. T.; Pugliese, M.; Bianco, G. V.; Bruno, G.; Nobile, C.; Carallo, S.; Fiore, A.; Sibillano, T.; Giannini, C.; et al. Electrochromic Evaluation of Airbrushed Water-Dispersible $W_{18}O_{49}$ Nanorods Obtained by Microwave-Assisted Synthesis. *Nanotechnology* **2021**, *32*, No. 215709.
(26) Mirzaei, A.; Neri, G. Microwave-Assisted Synthesis of Metal Oxide Nanostructures for Gas Sensing Application: A Review. *Sens. Actuators, B* **2016**, *237*, 749−775.
(27) Prontera, C. T.; Sico, G.; Montanino, M.; De Girolamo Del Mauro, A.; Tassini, P.; Maglione, M. G.; Minarini, C.; Manini, P. Sustainable, Fluorine-Free, Low Cost and Easily Processable Materials for Hydrophobic Coatings on Flexible Plastic Substrates. *Materials* **2019**, *12*, No. 2234.
(28) Chen, H.; Ding, X.; Pan, X.; Hayat, T.; Alsaedi, A.; Ding, Y.; Dai, S. Comprehensive Studies of Air-Brush Spray Deposition Used in Fabricating High-Efficiency CH3NH3PbI3 Perovskite Solar Cells: Combining Theories with Practices. *J. Power Sources* **2018**, *402*, 82−90.
(29) Chemseddine, A.; Moritz, T. Nanostructuring Titania: Control over Nanocrystal Structure, Size, Shape, and Organization. *Eur. J. Inorg. Chem.* **1999**, *1999*, 235−245.
(30) Bianco, G. V.; Sacchetti, A.; Milella, A.; Grande, M.; D'Orazio, A.; Capezzuto, P.; Bruno, G. Extraordinary Low Sheet Resistance of CVD Graphene by Thionyl Chloride Chemical Doping. *Carbon* **2020**, *170*, 75−84.
(31) Giannuzzi, R.; Primiceri, V.; Scarfiello, R.; Pugliese, M.; Mariano, F.; Maggiore, A.; Prontera, C. T.; Carallo, S.; De Vito, C.; Carbone, L.; Maiorano, V. Photochromic Textiles Based upon Aqueous Blends of Oxygen-Deficient WO3-x and TiO2 Nanocrystals. *Textiles* **2022**, *2*, 382−394.
(32) Cinquino, M.; Prontera, C. T.; Zizzari, A.; Giuri, A.; Pugliese, M.; Giannuzzi, R.; Monteduro, A. G.; Carugati, M.; Banfi, A.; Carallo, S.; et al. Effect of Surface Tension and Drying Time on Inkjet-Printed PEDOT:PSS for ITO-Free OLED Devices. *J. Sci.: Adv. Mater. Devices* **2022**, *7*, No. 100394.
(33) Majee, S.; Karlsson, M. C. F.; Wojcik, P. J.; Sawatdee, A.; Mulla, M. Y.; Alvi, N. u. H.; Dyreklev, P.; Beni, V.; Nilsson, D. Low Temperature Chemical Sintering of Inkjet-Printed Zn Nanoparticles for Highly Conductive Flexible Electronic Components. *npj Flexible Electron.* **2021**, *5*, No. 14.
(34) Darmawi, S.; Burkhardt, S.; Leichtweiss, T.; Weber, D. A.; Wenzel, S.; Janek, J.; Elm, M. T.; Klar, P. J. Correlation of Electrochromic Properties and Oxidation States in Nanocrystalline Tungsten Trioxide. *Phys. Chem. Chem. Phys.* **2015**, *17*, 15903−15911.
(35) Gu, H.; Guo, C.; Zhang, S.; Bi, L.; Li, T.; Sun, T.; Liu, S. Highly Efficient, Near-Infrared and Visible Light Modulated Electrochromic Devices Based on Polyoxometalates and W18O49 Nanowires. *ACS Nano* **2018**, *12*, 559−567.
(36) Xie, J.; Song, B.; Zhao, G.; Han, G. Citric Acid Induced W18O49 Electrochromic Films with Enhanced Optical Modulation. *Appl. Phys. Lett.* **2018**, *112*, No. 231902.
(37) Zhang, W.; Yue, L.; Zhang, F.; Zhang, Q.; Gui, X.; Guan, R.; Hou, G.; Xu, N. One-Step in Situ Synthesis of Ultrathin Tungsten Oxide@carbon Nanowire Webs as an Anode Material for High Performance. *J. Mater. Chem. A* **2015**, *3*, 6102−6109.
(38) Sun, Y.; Wang, W.; Qin, J.; Zhao, D.; Mao, B.; Xiao, Y.; Cao, M. Oxygen Vacancy-Rich Mesoporous W18O49 Nanobelts with Ultrahigh Initial Coulombic Efficiency toward High-Performance Lithium Storage. *Electrochim. Acta* **2016**, *187*, 329−339.
(39) Granqvist, C. G. *Handbook of Inorganic Electrochromic Materials*; Elsevier, 1995.
(40) Mortimer, R. J.; Rosseinsky, D. R.; Monk, P. M. S. *Electrochromism: Fundamentals and Applications*; Wiley-VCH, 2008.
(41) Mortimer, R. J.; Rosseinsky, D. R.; Monk, P. M. S. *Electrochromic Materials and Devices*; Wiley-VCH, 2015.
(42) Larsson, A.-L.; Sernelius, B. E.; Niklasson, G. A. Optical Absorption of Li-Intercalated Polycrystalline Tungsten Oxide Films: Comparison to Large Polaron Theory. *Solid State Ionics* **2003**, *165*, 35−41.
(43) Salje, E.; Güttler, B. Anderson Transition and Intermediate Polaron Formation in WO3-x Transport Properties and Optical Absorption. *Philos. Mag. B* **1984**, *50*, 607−620.


https://doi.org/10.1021/acssuschemeng.3c00865
ACS Sustainable Chem. Eng. 2023, 11, 9601−9612

(44) Hagfeldt, A.; Graetzel, M. Light-Induced Redox Reactions in Nanocrystalline Systems. *Chem. Rev.* **1995**, *95*, 49−68.
(45) Cantão, M. P.; Cisneros, J. I.; Torresi, R. M. Electrochromic Behaviour of Sputtered Titanium Oxide Thin Films. *Thin Solid Films* **1995**, *259*, 70−74.
(46) Giannuzzi, R.; Prontera, T.; Tobaldi, D. M.; Pugliese, M.; De Marco, L.; Carallo, S.; Gigli, G.; Pullar, R. C.; Maiorano, V. Pseudocapacitive Behaviour in Sol-Gel Derived Electrochromic Titania Nanostructures. *Nanotechnology* **2021**, *32*, No. 45703.
(47) Enright, B.; Fitzmaurice, D. Spectroscopic Determination of Electron and Hole Effective Masses in a Nanocrystalline Semiconductor Film. *J. Phys. Chem. A* **1996**, *100*, 1027−1035.
(48) van de Krol, R.; Goossens, A.; Meulenkamp, E. A. Electrical and Optical Properties of TiO2 in Accumulation and of Lithium Titanate Li0.5TiO2. *J. Appl. Phys.* **2001**, *90*, 2235−2242.
(49) Kang, T.; Kim, D.; Kim, K. Time-Dependent Electrochromism of Nanocrystalline TiO2 Films in Propylene Carbonate Solution of LiClO4. *J. Electrochem. Soc.* **1998**, *145*, 1982−1986.
(50) Primiceri, V.; Pugliese, M.; Prontera, C. T.; Monteduro, A. G.; Esposito, M.; Maggiore, A.; Cannavale, A.; Giannuzzi, R.; Gigli, G.; Maiorano, V. Low-Cost Gel Polymeric Electrolytes for Electrochromic Applications. *Sol. Energy Mater. Sol. Cells* **2022**, *240*, No. 111657.



https://doi.org/10.1021/acssuschemeng.3c00865
*ACS Sustainable Chem. Eng.* 2023, 11, 9601−9612